CONTINUOUS-WAVE INTERBAND PHOTOREFRACTION IN $Sn_2P_2S_6$

G. MONTEMEZZANI, R. RYF, D. HAERTLE, P. GÜNTER, A. A. GRABAR[1], I. M. STOIKA[1], Yu. M. VYSOCHANSKII[1]

UDC 535.215

Nonlinear Optics Laboratory, Swiss Federal Institute of Technology
(ETH Hönggerberg, CH-8093 Zürich, Switzerland; e-mail: montemezzani@nlo.ch),

[1]**Institute of Solid State Physics and Chemistry, Uzhgorod National University**
(88000 Uzhgorod, Ukraine; e-mail: agrabar@univ.uzhgorod.ua)

$Sn_2P_2S_6$ crystals are used to record fast dynamic holograms by means of photorefractive effects under continuous-wave interband illumination at wavelengths of 514 and 488 nm. First results indicating response times in the sub-millisecond regime are presented and discussed.

The conventional photorefractive effect [1–3] relies on a redistribution of bulk charges due to the carrier photoexcitation from some deep donor level of a semiconductor-like material to the conduction or valence band. The most interesting feature of this (indirect) nonlinear optical process is that it can occur at moderate light intensity levels of the order of 1 W/cm^2 or less. There is a price to pay for this, at any given moment in time, the density of carriers being in a movable state (in the conduction or valence band) is small as compared to the number of charges needed to be redistributed. The stationary space-charge field is usually reached only after multiple excitation, movement, and retrapping processes of the involved carriers. This leads to rather slow time responses that may range for common photorefractive materials between a fraction of a millisecond and several seconds or even minutes.

This problem can be partially overcomed if, instead of relying on light which is able to induce solely donor-to-band phototransitions, one uses highly absorbed light with the photon energy near electronic resonances, for which direct photransitions between the valence and conduction bands do occur. Even in the (ideal) total absence of deep traps, the charge separation and formation of a space-charge field are still possible if the mobilities of electrons and holes differ from each other [4]. It has been shown [4–7] that, with respect to conventional photorefractive gratings, such interband photorefractive gratings have three advantageous features. First, as mentioned above, they are built significantly faster as a consequence of the efficient photoexcitation (many charges are available in the valence band for being photoexcited). Second, since the charge modulation is stored mainly in the bands themselves or in their (energetical) vicinity, even an intense illumination at a wavelength which is unable to induce an interband transition does not affect the grating significantly. In other words, the interband photorefractive effect is very robust with respect to an intense flow of sub-bandgap photons. Third, in general, crystals do not need to be doped. In fact, interband gratings have usually a significantly higher sensitivity in undoped crystals than that in doped ones.

Tin hypothiodiphosphate ($Sn_2P_2S_6$, SPS) is a ferroelectric crystal with large electro-optic coefficients [8] and a moderate band-gap energy of 2.3 eV. In the conventional sense, this material exhibits very good photorefractive properties in the red and near infrared spectral ranges [9–14]. Since blue and green light is strongly absorbed, SPS is also an excellent candidate for the faster hologram recording via interband photorefraction in the visible. In the pulsed regime, effects ascribed to the interband photorefractive effect were already used to demonstrate optical correlation at high repetition frame rates using a wavelength of 532 nm [15, 16]. In this work, we discuss our first results on the recording of interband photorefractive gratings at green (λ = 514 nm) and blue (λ = 488 nm) wavelengths using continuous-wave illumination.

The $Sn_2P_2S_6$ crystal under investigation was cut along the pseudo-crystallographic axes and had a size of $X \times Y \times Z = 5.6 \times 5.9 \times 1.61$ mm^3. The spontaneous polarization is nearly parallel to the OX axis. We use the convention where the Y-axis is perpendicular to the crystallographic mirror plane, the X axis is parallel to the crystallographic a-axis, and the Z axis is perpendicular to X and Y, as described in [11]. The Z-faces were polished to high optical quality using colloidal fluids as a polishing medium.

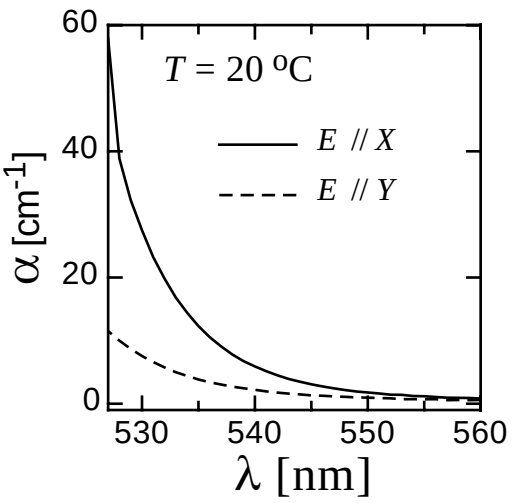

Fig. 1. Absorption spectrum of $Sn_2P_2S_6$ near the band-edge for light polarized along the X- or Y-axis

The absorption spectrum of $Sn_2P_2S_6$ near the band edge energy is shown in Fig. 1. The absorption edge is situated around the 530 nm wavelength. Note that, as expected, with increase in temperature, the absorption edge moves towards the infrared, and the absorption coefficient increases. For instance, for $\lambda = 532$ nm, the absorption constant for the X-polarization increases from ≈ 35 to 110 cm^{-1} between 25 and 50 °C. For shorter wavelengths the absorption constant increases rapidly following the Urbach behaviour [17]. At $\lambda = 488$ nm, recently published Urbach parameters [18] predict the absorption coefficients $\alpha_X = 1350 \pm 150\,cm^{-1}$ and $\alpha_Y = 2800 \pm 300\ cm^{-1}$.

For photoconductivity measurements, silver electrodes were painted on the X surfaces. Light propagating along the Z-direction is absorbed in the first layers behind the entrance surface and produces a spatially inhomogeneous current. The photoconductivity at a given illumination intensity I_0 can be evaluated by a differential method. Due to light absorption the light intensity $I(z)$ decreases exponentially in the direction of the surface normal z, that is $I(z) = I_0 \exp(-\alpha z)$. An increase of the incident intensity from I_0 to $I_0 + \Delta I_0$ leads to an effective shift of all the intensity distribution by the amount

$$\Delta z \approx \frac{1}{\alpha}\left(\frac{\Delta I_0}{I_0}\right) \qquad (1)$$

towards the bulk of the material. This forms a new effective conductive layer at the input surface associated with the intensity I_0 which contributes to the total current through the electrode surfaces. The additionally measured electrical current ΔI_{el} is then related to the increase ΔI_0 of the light intensity via the photoconductivity $\sigma_{ph}(I_0)$ of the additional layer, the latter can then be calculated as

$$\sigma_{ph}(I_0) = \frac{\alpha I_0}{bE}\frac{\Delta I_{el}}{\Delta I_0}, \qquad (2)$$

where b is the crystal dimension in the vertical Y direction and E is the applied electric field. If the photoconductivity is due solely to the interband photoexcitation and recombination processes, σ_{ph} is expected to increase proportionally to the square-root of the light intensity [4]. Figure 2 shows an example of curves $\sigma_{ph}(I_0)$ measured using the above-described method under a field of 200 V/cm. Illumination is at the wavelength $\lambda = 532$ nm which is still at the border of the high absorption region. Experiments for two different sample temperatures are shown. At the higher temperature (50 °C), where the absorption constant exceeds 100 cm^{-1}, the increase of the photoconductivity is described well by the relationship $\sigma_{ph}(I_0) \propto \sqrt{I_0}$ in the range of intensities above 1 mW/cm^2, as indicated by the dotted line. This suggests the likely interband nature of the process. At the lower temperature of 27 °C which is associated to a weaker absorption constant, in contrast, this regime is not yet reached at the intensities used here. This is probably due to the strong importance (in this experimental regime) of charge recombination processes involving deep traps. Note that, by decreasing the illumination wavelength to 514 or 488 nm, the room-temperature photoconductivity behaves similarly to the upper case of Fig. 2. For $I_0 > 1$ mW/cm^2, one finds always $\sigma_{ph}(I_0) \propto (I_0)^x$ with $x \approx 0.5$, i.e. a regime which is most likely dominated by interband processes.

Holographic investigations were performed in the longitudinal geometry [4], where the plane recording waves (being completely absorbed in the crystal) and the read-out wave at longer wavelengths share a common plane of incidence (in our case containing the axis Z). Due to the high absorption and the resulting limited effective thickness of the induced gratings, interband gratings recorded in this configuration are usually characterized by a rather low diffraction efficiency. In our case, the diffraction efficiency (measured by a red He—Ne beam at $\lambda = 633$ nm polarized in the XZ-plane) reaches up to $\eta = 0.16\%$ for Y-polarized recording beams at 514 nm (an intensity of 0.7 W/cm^2). At the same intensity, for p- (XZ-) polarization or for the shorter wavelength (488 nm) of the recording waves, the diffraction efficiency decreases by up to two orders of

magnitude, which we can attribute to a decrease of the effective grating thickness.

For elucidating the origin of recorded gratings, it is more important to study the dependence of diffraction properties on the direction of the grating vector $\vec{K}$. The latter can be rotated in the XY-plane by rotating the crystal around the Z-axis. In order to keep constant external conditions, the polarizations of all the involved recording and read-out beams have to be rotated as well, so that they have an unchanged direction in the crystalline system of coordinates. By such investigations, we have verified that no diffraction is observed in the case where the grating vector is parallel to the Y-axis, while a maximum in the diffraction efficiency is observed for a directions of the grating vector close to the X-axis of the crystal. Due to the absence of diagonal electro-optic coefficients of the type r_{ii2} in $Sn_2P_2S_6$ in the case where the grating is mediated by the electro-optic effect, isotropic Bragg diffraction is prohibited by symmetry for a grating vector in the Y-direction. On the other hand, if a modulated space-charge electric field with $\vec{K}||X$ does exist, then the effective electro-optic coefficient giving rise to a corresponding refractive index modulation is expected to significantly profit from the largest coefficients (r_{111}) measured for homogeneous fields [8].

The above discussion excludes phenomena such as absorption-type gratings which do not follow the same symmetry constraints and shows that the electro-optic response is a necessary feature for the observation of gratings. The physical mechanism at work is therefore likely to be the interband photorefractive effect in the sense discussed in [4]. In order to support this suggestion, we want nevertheless to discuss shortly the possible role played by other mechanisms as well.

One possible alternative mechanism is represented by space-charge gratings induced by the pyroelectric effect. Due to the strong light absorption of $Sn_2P_2S_6$ at 488 and 514 nm, the crystal temperature will locally change as a function of the incident light intensity when the light of the writing beams is turned on. The temperature dependence of the spontaneous polarization (pyroelectric effect) will generate a space charge field, which will be revealed by the electro-optic effect as a phase grating. This mechanism follows the same symmetry rules like the conventional or interband photorefractive effect and was investigated in detail by Ducharme [19] and Buse [20]. However, since the pyroelectric effect relies on a temperature change, the contributions due to this effect are usually significant only under high-intensity pulsed

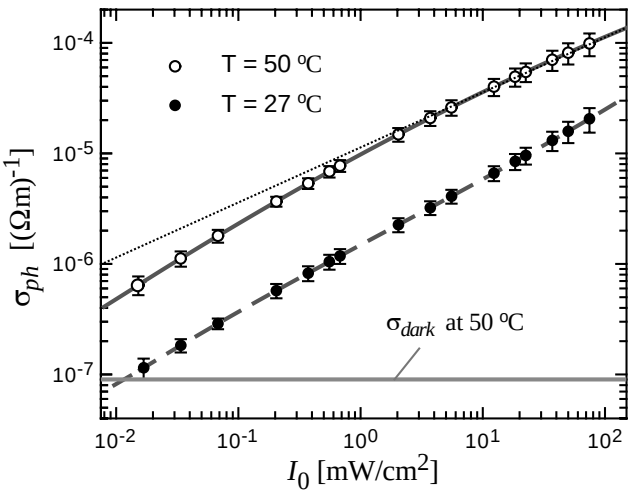

Fig. 2. Intensity dependence of the cw photoconductivity for illumination with X-polarized light at $\lambda = 532$ nm

illumination. In our low-intensity continuous-wave regime, these contributions are found to be irrelevant. Note that even for our earlier pulsed investigations using the wavelength 532 nm [16], the expected pyroelectric contribution to the diffraction efficiency is more than two orders of magnitude below the observed effects. This can be verified by using published values for the spontaneous polarization and specific heat of $Sn_2P_2S_6$ [21, 22] and indicates that this effect is not relevant in the experimental regimes we have used.

The strong light absorption and the consequent local heating of the sample may also produce directly a diffraction grating through the thermo-optical effect. The highest temperature change modulation ΔT is expected again for the short pulse excitation because, in this case, the temperature has not yet the time to partially homogenize by means of heat transport. In this case, the temperature change ΔT can be calculated as

$$\Delta T = \frac{1}{\tilde{c}} \alpha \Delta F_0, \tag{3}$$

where ΔF_0 is the fluence modulation of the writing beams and $\tilde{c}$ is the volume specific heat of the material. With $\Delta F_0 = 10 \mu$J/cm^2, $\tilde{c} = 0.83$ J/(cm^{3}K), and $\alpha = 30$ cm^{-1} (pulsed excitation at 532 nm), one obtains $\Delta T \approx 0.36$ mK. Due to heat transport, the temperature modulation for the case of cw illumination is even lower. By solving the heat diffusion equation with a driving term that takes into account the heat deposited by light absorption, one obtains the temperature modulation amplitude

$$\Delta T = \frac{\alpha \Delta I}{K^2 \kappa}, \tag{4}$$

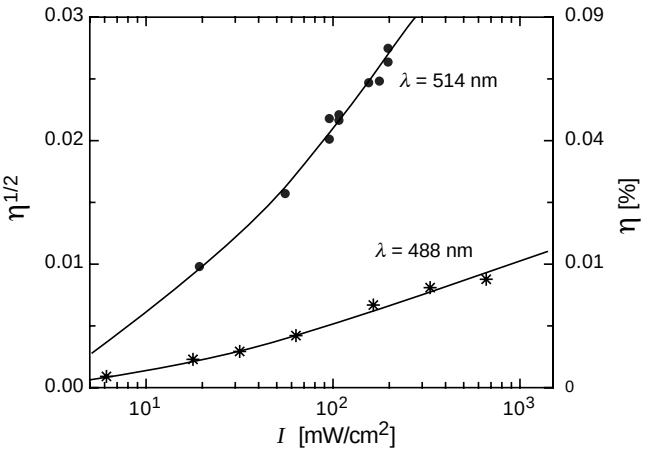

Fig. 3. Intensity dependence of the diffraction efficiency η measured in the longitudinal geometry for Y-polarized recording light at two wavelengths

where ΔI is the modulation amplitude of the light intensity, K is the grating vector and κ is the thermal conductivity which is about 0.5 W/(m K) for $Sn_2P_2S_6$ at room temperature [23]. Even for the highest absorption constant $\alpha_Y = 2800$ cm^{-1} (488 nm) and for $\Delta I = 100$ mW/cm^2, at a grating spacing of 1 μm, one expects a temperature modulation of only about $\Delta T \approx 0.014$ mK for the cw excitation. Note that, considering the temperature dependence of the refractive indices [24], a temperature modulation of 0.36 mK (pulsed regime) would give rise to a refractive index modulation of about $3.6 \cdot 10^{-7}$. This is almost two orders of magnitude below the experimentally measured one under such conditions. Furthermore, this value would be expected to be approximately the same for every direction of the grating vector, which clearly contradicts the above-mentioned observation of a vanishing diffraction for a grating vector in the Y direction.

Finally, we can exclude the importance of potential surface deformation gratings by the fact that the related multiple diffraction orders that would be expected for such gratings (Raman—Nath regime) were never observed.

It appears therefore that the observed diffraction is due to interband photorefractive gratings. If this is the case, the diffraction efficiency in the longitudinal geometry is expected to depend strongly on the light intensity I_0. In the most simplified model, one may assume that the effective grating thickness is increased by increasing the intensity, while the average refractive index change Δn remains unchanged [4]. For the diffraction efficiency, this leads to a dependence of the type $\sqrt{\eta} \propto (\Delta n/\alpha)\ln(I_0/I_{\rm ref})$, where $I_{\rm ref}$ is a reference intensity. This type of an increase would give a straight line in the coordinates chosen for Fig. 3 which depicts the intensity dependence of the diffraction efficiency upon recording at 514 and 488 nm. The data show a slight overlinear behavior in the chosen representation, which can be attributed to an increase of the (depth-averaged) refractive index change with increasing intensity.

As already mentioned, probably the most attractive property of interband photorefractive effects is their much faster dynamics as compared to conventional photorefraction. Fig. 4 shows an example of a dynamic behavior at $\lambda = 488$ nm for Y-polarization. The recording beams were turned on for 1 ms using an acousto-optic modulator with a response time of less than 1 μs. It can be observed that, during the build-up, the diffraction efficiency reaches a value close to the saturation value already after less than 100 μs. During a dark decay, the dynamics shows a fast initial decay in a time of the order of 10 μs, followed by a slower grating relaxation in a time of few milliseconds. The dynamics of the diffraction efficiency presented in Fig. 4 cannot be directly related to the theoretical space-charge field dynamics reported in [6, 25], because the intensity of the writing beam is exponentially decreasing as a function of the depth inside the crystal. For the build-up of the holographic grating, this means that the build-up time, the amplitude, and the phase of the grating will depend on the depth. In the longitudinal geometry, the diffracted beam at the back side of the crystal is formed by the coherent sum of all the amplitudes of the diffracted light at different depths, each evolving with a different dynamics.

The build-up was therefore modeled with a semi-heuristic double exponential build-up function of the form

$$\sqrt{\eta(t)} = \sqrt{\eta_1}(1-\exp(-t/\tau_1)) + \sqrt{\eta_2}(1-\exp(-t/\tau_2)), \quad (5)$$

which is plotted in Fig. 4,*b* and, even though not perfectly, follows the measured data in a satisfactory way. The parameters for this plot are $\tau_1 = 8.3$ μs for the fast time constant and $\tau_2 = 103$ μs for the slow one. The corresponding amplitudes are $\eta_1 = 2.8 \cdot 10^{-5}$ and $\eta_2 = 1.5 \cdot 10^{-5}$, respectively.

Note that, due to the robustness of interband gratings, the presence of the red read-out beam does almost not influence the grating written in the blue-green. This holds also for intensities of the red light which are much larger than the intensity of blue-green recording beams. However, for depths much larger than the typical penetration depth $d = 1/\alpha$ of the

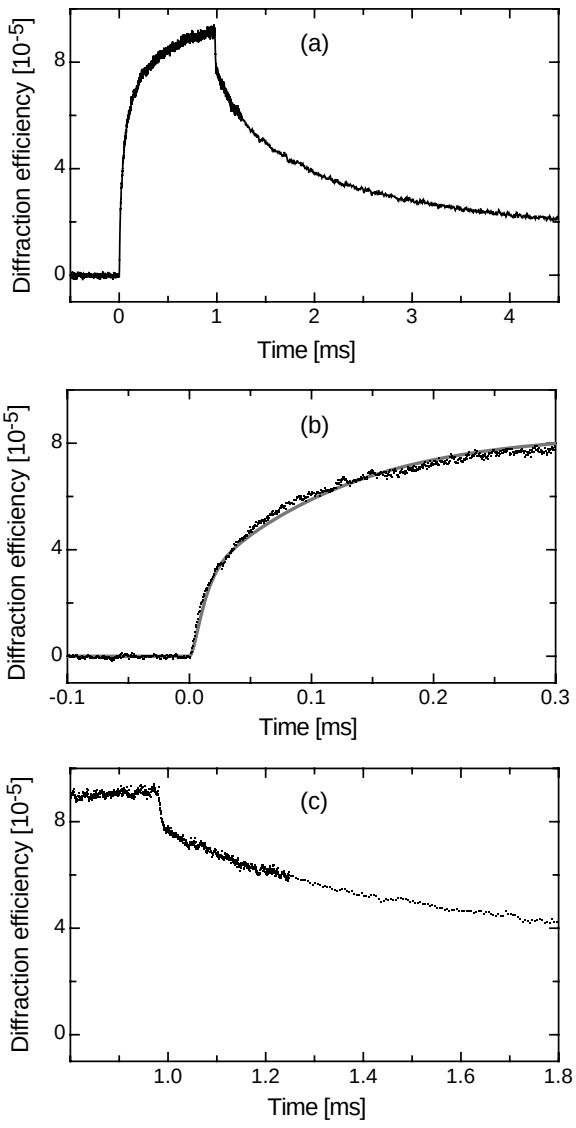

Fig. 4. Dynamics of diffraction for a grating recorded at the 488 nm wavelength (Y-polarization) with the intensity $I = 720$ mW/cm^2 and at the grating spacing $\Lambda = 1.4\mu$m. *a* — recording during 1 ms and subsequent dark decay; *b* and *c* — enlargement of the initial parts of the recording and decay curves, respectively. The solid line in (b) is a double exponential fit according to Eq. (5), see text

blue-green beams, a coupling of the diffracted and transmitted red beams can occur. This can be verified by repeating the experiment with opposite direction of the spontaneous polarization. In our experiment however, this effect was of practically no importance because the conventional photorefraction induced by red light is much slower than the interband processes involved here.

In conclusion, we have studied the holographic gratings recorded in $Sn_2P_2S_6$ crystals under cw interband illumination. The results of photoconductivity and Bragg diffraction investigations are consistent with a mechanism of grating formation involving the interband photorefractive effect. Grating build-up times of the order of 100 μs with a fast time constant shorter than 10 μs were observed for intensities less than 1 W/cm^2. $Sn_2P_2S_6$ may therefore prove as a very interesting material for the dynamic optical parallel processing in the blue-green spectral range.

We dedicate this article to Prof. Dr. Marat Soskin on the occasion of his 75th birthday. His contributions to holography and singular optics have inspired and stimulated the scientific community over several decades.

1. *Chen F.S., LaMacchia J.T., Fraser D.B.* // Appl. Phys. Lett. **13** (1968) 223.
2. *Kukhtarev N.V., Markov V.B., Odulov S.G. et al.* // Ferroelectrics **22** (1979) 949—960.
3. *Photorefractive* Materials and their Applications I: Fundamental Phenomena/Ed. by P. Günter, J.P. Huignard. — Vol. 1 of Topics in Applied Physics. — Berlin: Springer, 1988.
4. *Montemezzani G., Rogin P., Zgonik M., Günter P.* // Phys. Rev. B **49** (1994) 2484—2502.
5. *Montemezzani G., Rogin P., Zgonik M., Günter P.* // Opt. Lett. **18** (1993) 1144—1146 .
6. *Bernasconi P., Montemezzani G., Günter P.* // Appl. Phys. B **68** (1999) 833—842.
7. *Montemezzani G., Bernasconi P., Dittrich P. et al.* // Proc. SPIE **4358** (2001) 1—10.
8. *Haertle D., Caimi G., Haldi A. et al.* // Opt. Communs. **215** (2003) 333—343.
9. *Grabar A.A.* // Ferrolelectrics **170** (1995) 133—137.
10. *Odoulov S.G., Shumelyuk A.N., Hellwig U. et al.* // Opt. Lett. **21** (1996) 752—754.
11. *Odoulov S.G., Shumelyuk A.N., Hellwig U. et al.* // J. Opt. Soc. Amer. B **13** (1996) 2352—2360.
12. *Grabar A.A., Kedyk I.V., Gurzan M.I. et al.* // Opt. Communs. **188** (2001) 187—194.
13. *Shumelyuk A., Odoulov S., Kip D., Krätzig E.* // Appl. Phys. B **72** (2001) 707—710.
14. *Jazbinsek M., Montemezzani G., Günter P. et al.* // J. Opt. Soc. Amer. B **20** (2003) 1241—1246.
15. *Ryf R., Montemezzani G., Günter P. et al.* // Trends Opt. Photon. **62** (2001) 11—17.
16. *Ryf R., Montemezzani G., Günter P. et al.* // Opt. Lett. **26** (2001) 1666—1668.
17. *Urbach F.* // Phys. Rev. **92** (1953) 1324.
18. *Studenyak I.P., Mitrovcij V.V., Kovacs Gy.Sh. et al.* // Ferroelectrics **254** (2001) 295—310.

19. *Ducharme S.* // Opt. Lett. **16** (1991) 1791—1793.

20. *Buse K.* // J. Opt. Soc. Amer. B **10** (1993) 1266—1275.

21. *Moriya K., Kuniyoshi H., Tashita K. et al.* // J. Phys. Soc. Jpn. **67** (1998) 3505—3511.

22. *Maĭor M.M., Koperles B.M., Savchenko B.A. et al.* // Sov. Phys. Solid State **25** (1983) 117.

23. *Al'Shufi K., Rizak V.M., Rizak I.M. et al.* // Phys. Solid State **35** (1993) 1055—1057.

24. *Grabar A.A., Vysochanskii Yu.M., Perechinskii S.I. et al.* // Sov. Phys. Solid State **26** (1984) 2087—2089.

25. *Bernasconi P., Montemezzani G., Biaggio I., Günter P.* // Phys. Rev. B **56** (1997) 12196—12200.

МІЖЗОННА ФОТОРЕФРАКЦІЯ В КРИСТАЛАХ $Sn_2P_2S_6$ ПІД ДІЄЮ НЕПЕРЕРВНОГО ЛАЗЕРНОГО ВИПРОМІНЮВАННЯ

Г. Монтемеццані, Р. Руф, Д. Хаертле, П. Гюнтер, А.А. Грабар, І.М. Стойка, Ю.М. Височанський

Р е з ю м е

Кристали $Sn_2P_2S_6$ використовуються для запису швидких динамічних голограм за допомогою фоторефрактивного ефекту при опроміненні неперервним лазерним випромінюванням з довжинами хвиль 514 та 488 нм. Представлено та обговорено перші результати, які свідчать про наявність часового відгуку в субмілісекундному режимі.